DOI: 10.19884/j.1672-5220.202404001

Design of Dual-Wavelength Bifocal Metalens Based on Generative Adversarial Network Model

LIU Gangcheng[1], WANG Junkai[1], LIN Sen[1], WU Binhe[1*], WANG Chunrui[1], ZHOU Jian[2], SUN Hao[2*]
1. College of Physics, Donghua University, Shanghai 201620, China
2. Shanghai Institute of Microsystem and Information Technology, Chinese Academy of Sciences, Shanghai 200050, China

Abstract: Multifocal metalenses are of great concern in optical communications, optical imaging and micro-optics systems, but their design is extremely challenging. In recent years, deep learning methods have provided novel solutions to the design of optical planar devices. Here, an approach is proposed to explore the use of generative adversarial networks (GANs) to realize the design of metalenses with different focusing positions at dual wavelengths. This approach includes a forward network and an inverse network, where the former predicts the optical response of meta-atoms and the latter generates structures that meet specific requirements. Compared to the traditional search method, the inverse network demonstrates higher precision and efficiency in designing a dual-wavelength bifocal metalens. The results will provide insights and methodologies for the design of tunable wavelength metalenses, while also highlighting the potential of deep learning in optical device design.

Keywords: generative adversarial network (GAN); metalens; forward network; inverse design
CLC number: O43 **Document code**: A
Article ID: 1672-5220(2025)02-0168-09

Open Science Identity (OSID)

0 Introduction

Metasurfaces, the two-dimensional equivalent of metamaterials, are artificially designed planar optical structures[1]. Metasurfaces are composed of the meta-atoms arranged periodically at subwavelength scales[2]. Tailored manipulation[3-5] targeting specific wavelengths or bands can be achieved through the modification of material properties, thicknesses, geometric parameters and arrangements of meta-atoms. Compared to traditional optical devices, metasurfaces exhibit higher flexibility, compactness and multifunctionality. Therefore, numerous optical components based on metasurfaces have been numerically simulated and experimentally validated, including vortex beams[6-8], holographic imaging[9-10], spectral filtering[11-12], metalenses[13-16] and polarization converters[17-18].

However, in the fields such as optical communications, optical imaging and micro-optics systems, metasurfaces are typically designed to operate at a single wavelength. To achieve independent control of metasurfaces at different wavelengths, researchers have conducted extensive studies. Xu et al.[19] optimized the structural parameters of the silicon nanorods by using a global optimization algorithm. They established a database covering all phase requirements for two wavelengths, allowing the reconstruction of different holograms for 532 nm x-linear-polarized light and 633 nm y-linear-polarized light. This method can greatly improve the design efficiency and minimize the cross-talk, but at the cost of time and computational resources. Arbabi et al.[20] proposed and experimentally demonstrated two-photon fluorescence microscopy with a dual-wavelength metalens working as the objective lens, enabling simultaneous focusing of different wavelengths and improved compactness. Nevertheless, it is currently not feasible to achieve imaging of two wavelengths at arbitrary positions on the focal plane. Qu et al.[21] demonstrated that, based on the principle of geometric phase modulation, two different types of meta-atoms could be arranged in different subregions to control the focusing performance of two wavelengths. Indeed, employing different types of meta-atoms to control the focusing of two wavelengths could result in inefficient use of design space.

In recent years, significant progress has been made in the field of acquiring target meta-atom structures by using deep learning[22-26], particularly with the use of generative adversarial networks (GANs)[27]. GANs consist of two mutually adversarial neural networks, known as the generator and the discriminator, respectively. Based on the original principles of GANs, researchers have proposed a number of GAN variants[28-31] showing outstanding performance in the field of inverse

Received date: 2024-04-01
Foundation item: National Natural Science Foundation of China (No. 61975029)
* Correspondence should be addressed to WU Binhe, email: bhwu@dhu.edu.cn; SUN Hao, email: sh@mail.sim.ac.cn
Citation: LIU G C, WANG J K, LIN S, et al. Design of dual-wavelength bifocal metalens based on generative adversarial network model[J]. *Journal of Donghua University (English Edition)*, 2025, 42(2): 168-176.

design for meta-atom structures. An et al.[32] proposed an approach for designing free-form all-dielectric metasurface devices by combining conditional generative adversarial networks (CGANs) and Wasserstein generative adversarial networks (WGANs). Through the inverse networks, they successfully validated optical devices such as a bifocal lens, a polarization-multiplexed deflector, a polarization-multiplexed lens and a polarization-independent lens, demonstrating the versatility of the method.

In this work, we present a design approach based on conditional Wasserstein generative adversarial network-gradient penalty (CWGAN-GP)[33-34] to achieve an efficient and precise design of a dual-wavelength bifocal metalens. The entire design process consists of a forward network and an inverse network. The forward network would rapidly predict the optical response of the meta-atom structure, while the inverse network would generate meta-atom structures that match the optical response. It is learned that current machine learning models perform well only for in-distribution inverse design, where the target optical response should align with the distribution of the training dataset[35]. However, the reality is that the target optical responses often do not conform to the distribution of the dataset. To address this issue, a method is proposed to search for curves in an untrained dataset that closely matches the target optical response and input them into the inverse network. The method is compared to a traditional search method. It is expected that the method would solve the problem of in-distribution and enhance the stability of the network.

1 Theoretical Model

1.1 Training dataset

An et al.[32] indicated that placing thin films with higher refractive indices on substrates with lower refractive indices would enhance the manipulation of light. Without loss of generality, to increase the phase freedom of the dual-wavelength bifocal metalens, the "needle-drop" approach is employed to generate various free-form structures of meta-atoms. The general structure of the meta-atom is shown in Fig. 1, which consists of a free-form silicon pattern and a silicon dioxide substrate, colored in cyan and gray, respectively. The thicknesses of the pattern and the substrate are 982.5 and 800.0 nm, respectively. Each meta-atom has a period of 1 280 nm. Images of free-form structural patterns and their corresponding optical responses are included within the dataset. The shapes of the meta-atoms are described by 32 pixel × 32 pixel images. In the 32 × 32 matrix representation, a pixel value of 0 represents the portion covered by vacuum, while a pixel value of 1 represents the absence of the silicon material. The selected optical response is the complex transmission coefficient S_{21} in the infrared wavelength range (2 400 to 3 000 nm), with 121 uniformly distributed wavelength points. Each transmission coefficient has real and imaginary parts, resulting in a spectral response vector size of 242 × 1. The finite-difference time-domain (FDTD) methodology is employed for the numerical simulation. Periodic boundary conditions are applied in the x and y directions, while perfectly matched layers (PMLs) are used on the z boundary. A y-polarized plane wave is incident upon the metasurface from the + z direction.

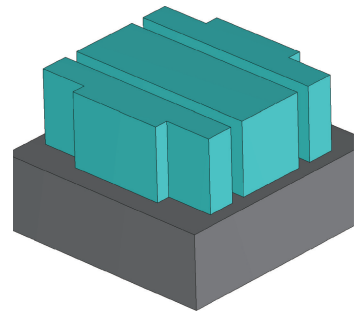

Fig. 1 General structural diagram of meta-atom

1.2 Forward network

The training dataset for the forward network consists of structural images of meta-atoms and their corresponding real and imaginary parts of the complex transmission coefficients. It is further divided into training, validation and test sets. This division enables robust model generalization and comprehensive performance evaluation. Moreover, a mean square error (MSE) serves as the loss function for the forward network, aiming to assess the difference between the target value and the predicted value.

$$L_{\text{pre}} = \frac{1}{N}\sum_{i=1}^{N}(Y_i - Y_i')^2, \tag{1}$$

where L_{pre} is the loss function; Y_i is the target value; Y_i' is the predicted value; N is the number of data.

The loss function calculates the partial derivatives of the model parameters, and uses the gradient descent algorithm to update the model weights in the parameter space along the opposite direction of the gradient. As the number of training times increases, the loss function gradually decreases and the model gradually fits the training data. Continuously adjusting the model weight parameters to minimize the loss function or reduce the difference between the target value and the predicted value is the goal of the entire process. The whole architecture model of the forward network consists of eight convolutional layers, four pooling layers and three fully connected layers, as shown in Fig. 2. The model fits best when there are eleven layers in our model. There are batch normalization layers and ReLU activation functions with max-pooling layers interleaved between every other convolutional layer. These light yellow modules represent the convolutional and fully connected layers, yellow modules indicate the batch normalization layers, light blue modules signify the activation function layers, and the red modules represent the max-pooling layers.

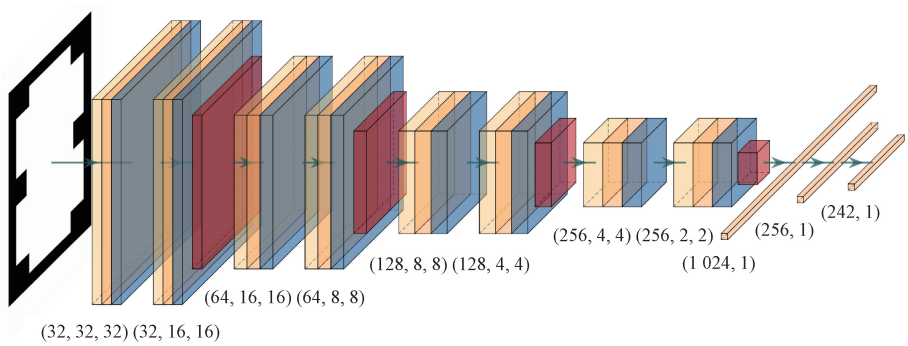

Fig. 2 Architecture of forward network

1.3 Inverse network

Using the CWGAN-GP method to reversely design the target spectrum has many advantages. On the one hand, compared with traditional GANs, CWGAN-GP uses the Wasserstein distance to distinguish images, resulting in more accurate results. On the other hand, the gradient penalty makes the entire inverse network more stable and can achieve outstanding convergence in a shorter training time. In terms of training methods, the discriminator is trained three times and the generator is trained once. It should be noted that the GAN model is trained on a dataset composed of 30 000 meta-atoms. The proposed inverse network trains a generator G that maps a set of design conditions, $\boldsymbol{x} = [\mathrm{Re}(S_{21})\ \mathrm{Im}(S_{21})]$, combined with a noise vector $\boldsymbol{z}$ to produce a target design $\boldsymbol{y}'$. Herein $\boldsymbol{y}' = G(\boldsymbol{z} \mid \boldsymbol{x})$. The discriminator D calculates the Wasserstein distance between the real samples $\boldsymbol{y}$ and $\boldsymbol{y}'$, and it inversely tunes the parameters within the generator/discriminator network to minimize/maximize the Wasserstein distance by using a gradient algorithm. The optimization function is

$$(P_{\mathrm{data}}, P_G) \approx \max_D \left\{ E_{\boldsymbol{y}\sim P_{\mathrm{data}}}[D(\boldsymbol{y} \mid \boldsymbol{x})] - E_{\boldsymbol{y}'\sim P_G}[D(\boldsymbol{y}' \mid \boldsymbol{x})] - \lambda E_{\hat{R}\sim P_{\hat{R}}}[\max(0, \| \nabla_{\hat{R}} D(\widehat{R \mid \boldsymbol{x}}) \| - 1)] \right\}, \quad (2)$$

$$\hat{R} = \tau \times \boldsymbol{y} + (1 - \tau) \times \boldsymbol{y}', \quad (3)$$

where P_{data} is the distribution of real sample data; P_G is the distribution of generated sample data; $\hat{R}$ is the interpolation between real and fake samples; τ is any real number between 0 and 1; $E_{\boldsymbol{y}\sim P_{\mathrm{data}}}[D(\boldsymbol{y} \mid \boldsymbol{x})]$ denotes the discriminator's expectation over the real data distribution; $E_{\boldsymbol{y}'\sim P_G}[D(\boldsymbol{y}' \mid \boldsymbol{x})]$ denotes the discriminator's expectation over the fake data distribution; $\lambda E_{\hat{R}\sim P_{\hat{R}}}[\max(0, \| \nabla_{\hat{R}} D(\widehat{R \mid \boldsymbol{x}}) \| - 1)]$ is a gradient penalty term used to enforce the Lipschitz continuity condition on the discriminator and λ is a hyperparameter controlling the strength of the penalty.

It has been discerned from relevant studies that the current machine learning models can only work well for an in-distribution inverse design where the target optical responses should follow a similar distribution of the training dataset. However, when designing the metalens, target optical responses often do not conform to a similar distribution. One possible approach is to select the optical response closest to the target value from the untrained dataset and input it into the network to ensure a similar distribution. Subsequently, the inverse network generates multiple structures that meet the target optical response. There is a high probability that these structures will satisfy the phase information of the dual-wavelength bifocal metalens. Figure 3 illustrates the entire design architecture.

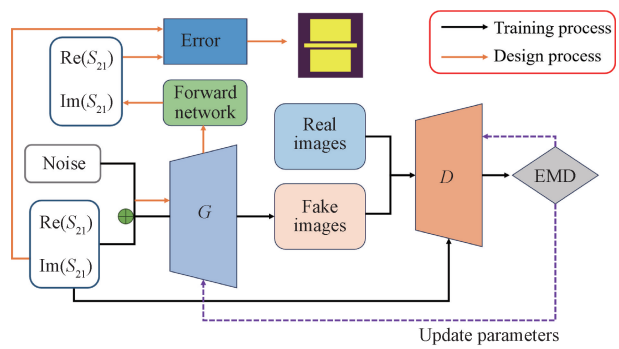

EMD—earth mover's distance.

Fig. 3 Training process of neural network model and reverse design process of metasurface

2 Design of Dual-Wavelength Bifocal Metalens

2.1 Forward network training and prediction results

In general, both the quantity and quality of training samples have a significant impact on the performance of deep learning models. When the number of training samples is either too small or too large, it can lead to inaccurate predictions. To highlight the predictive capability of the forward network, the training set consists of 60 000 samples, while the validation and test datasets each contain 4 000 samples. During the training process, numerous hyperparameters were evaluated. Ultimately, a batch size of 64 and a learning rate of 1×10^4 were selected, with the Adam optimizer being employed for weight training and optimization.

The training and validation loss curves during the training process of the forward network are displayed in Fig. 4. At 5 000 epochs, both curves converge smoothly, indicating the successful completion of the prediction task for the optical response of the meta-atom structures by the forward network.

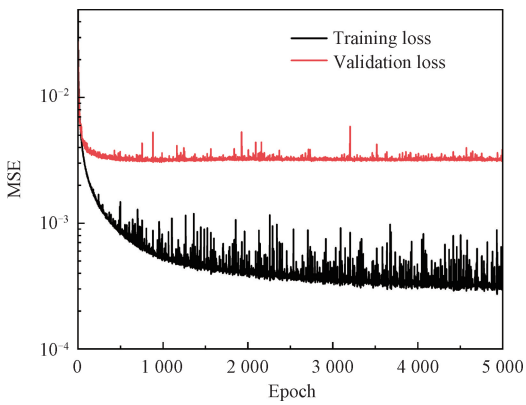

Fig. 4 Loss curves during training process of forward network

To demonstrate the model generalization ability to new data, the untrained test set was used for predictions. Since the real and imaginary parts of the complex transmission coefficients are contained in the output of the forward network, they are converted into amplitude and phase:

$$S_{\mathrm{amp}} = \sqrt{\mathrm{Im}(S_{21})^2 + \mathrm{Re}(S_{21})^2}, \tag{4}$$

$$S_{\mathrm{pha}} = \arctan \frac{\mathrm{Im}(S_{21})}{\mathrm{Re}(S_{21})}, \tag{5}$$

where S_{amp} is the amplitude; S_{pha} is the phase.

Figure 5 shows the comparison between the predicted results for the forward network and the numerically simulated results for four structures (shown in the insets). It can be clearly seen that the curves predicted by the forward network for the meta-atoms are almost identical to those of the simulated results. Hence, the excellent predictive performance of the forward network would contribute significantly to the design of a dual-wavelength bifocal metalens.

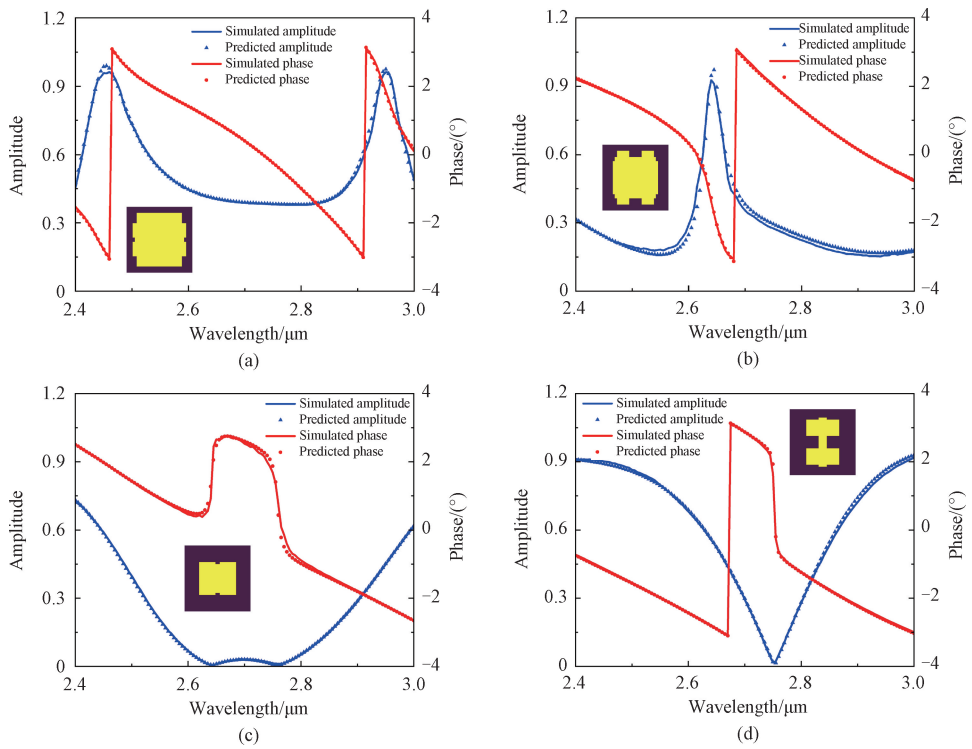

Fig. 5 Comparisons of predicted and numerically simulated amplitude-phase curves

2.2 Design results of dual-wavelength bifocal metalens

Our design goal is to achieve focusing at different positions on the focal plane with a focal length of 30 μm at two wavelengths. As shown in Fig. 6, the blue arrow indicates the propagation path of light at a wavelength of 2.4 μm. After modulation by the meta-atoms, the light focuses on the first quadrant. Similarly, the orange arrow represents the propagation path of light at a wavelength of 2.8 μm, with its focal point located in the third quadrant. Depending on the focal position, we can clearly distinguish different wavelengths. In the initial design phase, it is critical to calculate the phase profiles

on the metalens, as they define the phase distribution across the surface. The theoretical phase profiles at different wavelengths are shown in Fig. 7, with a phase range from 0 to 2π. The theoretical phase profile is calculated by

$$\varphi_m(x,y)=\frac{2\pi}{\lambda_m}\left(f-\sqrt{(x-x_1)^2+(y-y_1)^2+f^2}\right),\quad m=1,2, \tag{6}$$

where $\varphi_m(x,y)$ is the theoretical phase profile; λ_m is the wavelength; f is the focal length; (x_1, y_1) is the coordinate position of the focus. According to the phase information, meta-atoms that meet the phase conditions are arranged into a 31 × 31 square matrix. The final size of the metalens is 39.68 μm × 39.68 μm.

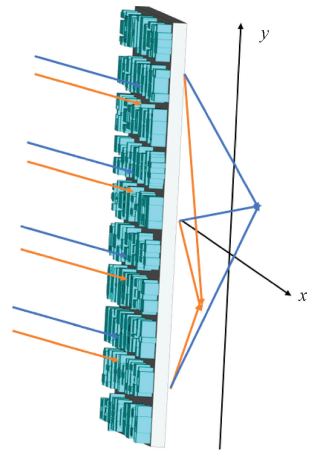

Fig. 6 Schematic diagram of dual-wavelength bifocal metalens

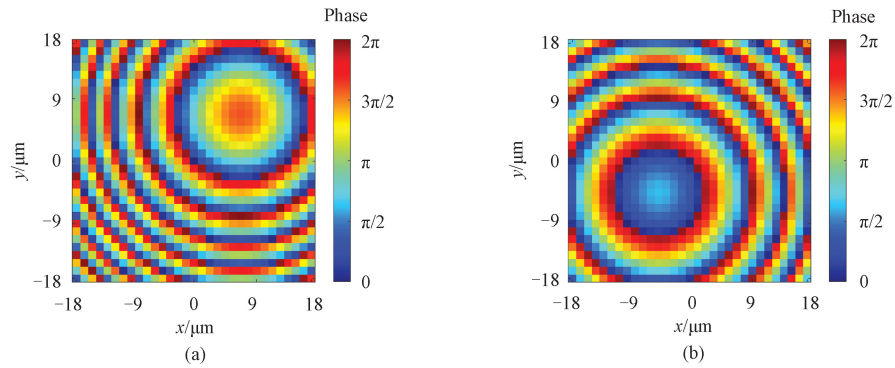

Fig. 7 Theoretical phase profiles of dual-wavelength bifocal metalens at different wavelengths: (a) 2.4 μm; (b) 2.8 μm

The workflow for designing the dual-wavelength bifocal metalens is as follows. Firstly, calculate the target phase profiles at two wavelengths. Secondly, select the optical response curve that is closest to the theoretical value from the untrained dataset, input it into the inverse network to generate multiple structural patterns, and perform symmetry processing. Thirdly, use the generated patterns as input to the forward network to obtain their optical responses in a short time. Finally, filter and array these meta-atoms to determine the structure of the metalens. The results of two examples are shown in Fig. 8. Figures 8(a) and 8(c) present 25 meta-atom structures generated to meet different target responses for examples 1 and 2, respectively. Figures 8(b) and 8(d) represent the amplitude and phase distributions of these structures at different wavelengths for examples 1 and 2, respectively, where the red solid line is the theoretically calculated phase at a wavelength of 2.4 μm, and the blue solid line is the theoretically calculated phase at a wavelength of 2.8 μm. In each polar plot, two red dots represent the amplitude and phase values of the input target curve at two wavelengths. Obviously, they are respectively close to the two target phase values. Near the red dots, the surrounding black dots represent the predicted amplitudes and phases at different wavelengths for the meta-atom structures generated by the inverse network. Since we only consider phase information, the structure closest to the theoretical phase is selected as the component of the metalens from the structures corresponding to the black points.

To demonstrate the superiority of deep learning over the traditional search method, a comparative analysis was conducted. The traditional search method relies on the dataset to query target meta-atoms, which not only fails to generate new structures but also heavily depends on the diversity of the dataset for its search results. When the dataset lacks certain specific types of structures, this method may be unable to effectively explore and generate these structures. Therefore, the search process requires substantial computational resources and time, leading to high computational costs and low search efficiency. Figures 9(a) and 9(b) depict the normalized light intensity distribution of the dual-wavelength bifocal metalens at the focal plane generated by the traditional search method. Figures 9(c) and 9(d) depict the normalized light intensity distribution of the dual-wavelength bifocal metalens at the focal plane generated by deep learning. It is clearly observed that the metalens generated by deep learning has a better focusing effect and a more accurate focusing position.

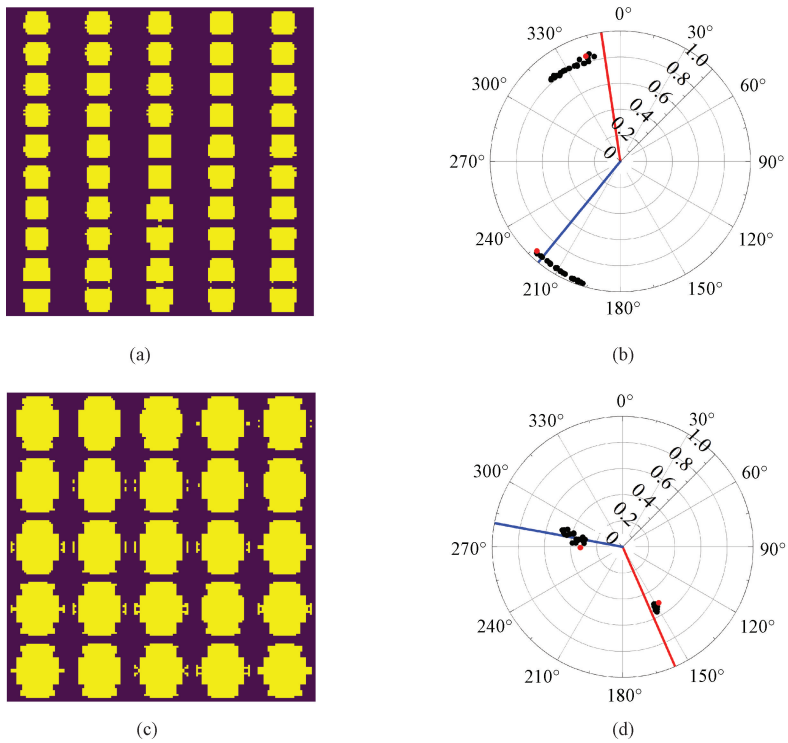

Fig. 8 Comparisons of predicted results and target values of meta-atoms generated by inverse network: (a) meta-atoms generated by inverse network of example 1; (b) amplitude and phase distributions at two wavelengths of example 1; (c) meta-atoms generated by inverse network of example 2; (d) amplitude and phase distributions at two wavelengths of example 2

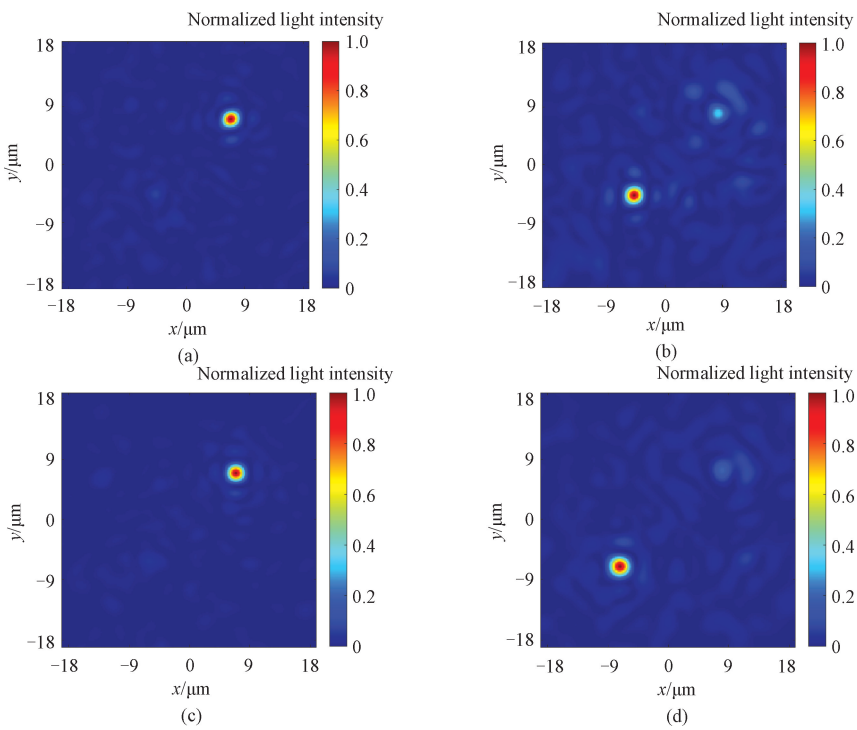

Fig. 9 Comparisons of normalized light intensity for dual-wavelength bifocal metalens designed: (a) 2.4 μm by traditional search method; (b) 2.8 μm by traditional search method; (c) 2.4 μm by deep learning; (d) 2.8 μm by deep learning

A clearer comparison method is to observe the focus intensity distribution along the x and z directions. Figures 10(a) and 10(b) illustrate the normalized light intensity distribution along the x and z directions at

wavelengths of 2.4 μm and 2.8 μm. The result of the deep learning shows a higher light intensity and a higher accuracy. At both wavelengths, the dual-wavelength bifocal metalens generated by the inverse network exhibits a more pronounced and concentrated light intensity distribution, emphasizing the excellence of the inverse network. With the learning and optimization capabilities of neural networks, deep learning can not only automatically learn the relationship between complex meta-atom structures and optical responses but also improve the accuracy and efficiency of reverse design. Therefore, the deep learning exhibits greater flexibility and intelligence in optical device design.

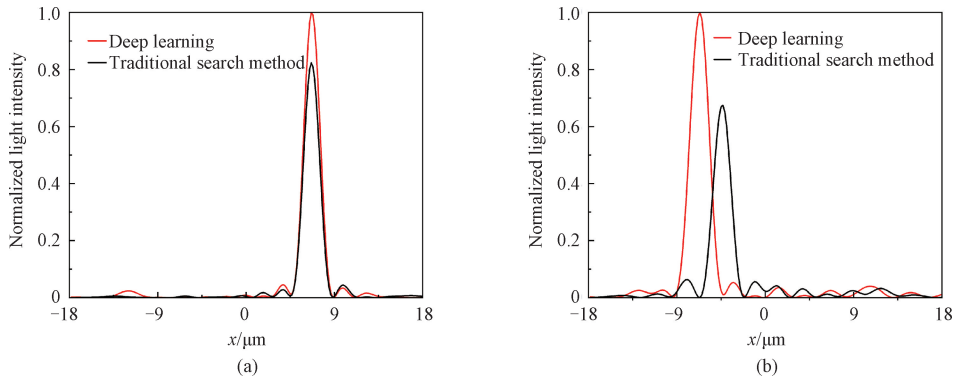

Fig. 10 Comparisons of normalized light intensity along x and z directions at different wavelengths: (a) 2.4 μm; (b) 2.8 μm

3 Conclusions

A deep generative adversarial network composed of a forward network and an inverse network is proposed for designing a dual-wavelength bifocal metalens, which is capable of rapidly generating meta-atoms to meet phase requirements at two wavelengths. Taking into account the advantages of current deep learning methods in in-distribution inverse design, the method that directly selects optical responses closest to the target values from the untrained dataset as inputs to the inverse network has been proposed. Compared with the traditional search method, the dual-wavelength bifocus metalens designed by the reverse network has a better focusing effect in terms of light intensity and a more accurate design target position. To achieve the design goal, the method still needs to rely on the original dataset. In the future, we would further explore the application of deep generative models to optical design, focusing particularly on developing improved methods to address situations where inverse design models cannot be directly applied.

References

[1] YU N F, GENEVET P, KATS M A, et al. Light propagation with phase discontinuities: generalized laws of reflection and refraction[J]. *Science*, 2011, 334(6054): 333-337.

[2] KIM J, YANG Y, BADLOE T, et al. Geometric and physical configurations of meta-atoms for advanced metasurface holography[J]. *InfoMat*, 2021, 3(7): 739-754.

[3] YU Y F, ZHU A Y, PANIAGUA-DOMÍNGUEZ R, et al. High-transmission dielectric metasurface with 2π phase control at visible wavelengths[J]. *Laser & Photonics Reviews*, 2015, 9(4): 412-418.

[4] OVERVIG A C, SHRESTHA S, MALEK S C, et al. Dielectric metasurfaces for complete and independent control of the optical amplitude and phase[J]. *Light: Science & Applications*, 2019, 8: 92.

[5] WANG H L, MA H F, CHEN M, et al. A reconfigurable multifunctional metasurface for full-space control of electromagnetic waves[J]. *Advanced Functional Materials*, 2021, 31(25): 2100275.

[6] YUE F Y, WEN D D, XIN J T, et al. Vector vortex beam generation with a single plasmonic metasurface[J]. *ACS Photonics*, 2016, 3(9): 1558-1563.

[7] ZHANG L, LI J S. Vortex beam generator working in terahertz region based on transmissive metasurfaces[J]. *Optik*, 2021, 243: 167452.

[8] AHMED H, KIM H, ZHANG Y B, et al. Optical metasurfaces for generating and manipulating optical vortex beams[J]. *Nanophotonics*, 2022, 11(5): 941-956.

[9] HUANG L L, ZHANG S, ZENTGRAF T. Metasurface holography: from fundamentals to applications[J]. *Nanophotonics*, 2018, 7(6): 1169-1190.

[10] NI X J, KILDISHEV A V, SHALAEV V M. Metasurface holograms for visible light[J]. *Nature Communications*, 2013, 4: 2807.

[11] PARK C S, SHRESTHA V R, YUE W J, et al. Structural color filters enabled by a dielectric metasurface incorporating hydrogenated amorphous silicon nanodisks[J]. *Scientific*

Reports, 2017, 7: 2556.
[12] HAN X, FAN Z Y, LIU Z Y, et al. Inverse design of metasurface optical filters using deep neural network with high degrees of freedom[J]. *InfoMat*, 2021, 3(4): 432-442.
[13] KHORASANINEJAD M, CHEN W T, DEVLIN R C, et al. Metalenses at visible wavelengths: diffraction-limited focusing and subwavelength resolution imaging [J]. *Science*, 2016, 352 (6290): 1190-1194.
[14] CHEN W T, ZHU A Y, SANJEEV V, et al. A broadband achromatic metalens for focusing and imaging in the visible [J]. *Nature Nanotechnology*, 2018, 13: 220-226.
[15] ARBABI A, FARAON A. Advances in optical metalenses[J]. *Nature Photonics*, 2023, 17: 16-25.
[16] YANG M Y, SHEN X, LI Z P, et al. High focusing efficiency metalens with large numerical aperture at terahertz frequency [J]. *Optics Letters*, 2023, 48(17): 4677.
[17] POUYANFAR N, NOURINIA J, GHOBADI C. Multiband and multifunctional polarization converter using an asymmetric metasurface[J]. *Scientific Reports*, 2021, 11: 9306.
[18] WANG P, ZHANG Y, WANG Y, et al. Multifunctional polarization converter based on multilayer reconfigurable metasurface [J]. *Defence Technology*, 2023, 28: 136-145.
[19] XU P, XIAO Y F, HUANG H X, et al. Dual-wavelength hologram of high transmittance metasurface[J]. *Optics Express*, 2023, 31(5): 8110.
[20] ARBABI E, LI J Q, HUTCHINS R J, et al. Two-photon microscopy with a double-wavelength metasurface objective lens[J]. *Nano Letters*, 2018, 18(8): 4943-4948.
[21] QU J Q, LUO H J, YU C Y. Dual-wavelength polarization-dependent bifocal metalens for achromatic optical imaging based on holographic principle[J]. *Sensors*, 2022, 22(5): 1889.
[22] AN S S, FOWLER C, ZHENG B W, et al. A deep learning approach for objective-driven all-dielectric metasurface design [J]. *ACS Photonics*, 2019, 6(12): 3196-3207.
[23] NOH J, NAM Y H, SO S, et al. Design of a transmissive metasurface antenna using deep neural networks[J]. *Optical Materials Express*, 2021, 11(7): 2310.
[24] FOWLER C, AN S, ZHENG B, et al. Deep learning for metasurfaces and metasurfaces for deep learning[M]//Advances in Electromagnetics Empowered by Artificial Intelligence and Deep Learning. New York, USA: IEEE, 2023: 319-343.
[25] AN S S, ZHENG B W, SHALAGINOV M Y, et al. Deep learning modeling approach for metasurfaces with high degrees of freedom [J]. *Optics Express*, 2020, 28(21): 31932.
[26] NADELL C C, HUANG B H, MALOF J M, et al. Deep learning for accelerated all-dielectric metasurface design [J]. *Optics Express*, 2019, 27(20): 27523.
[27] WANG J K, LIN S, LIU G C, et al. Reverse design of metasurface based on generative adversarial network model [J]. *Journal of Donghua University (Natural Science)*, 2024, 50(5): 61-68. (in Chinese)
[28] YEUNG C, TSAI R, PHAM B, et al. Global inverse design across multiple photonic structure classes using generative deep learning [J]. *Advanced Optical Materials*, 2021, 9 (20): 2100548.
[29] KIANI M, KIANI J, ZOLFAGHARI M. Conditional generative adversarial networks for inverse design of multifunctional metasurfaces [J]. *Advanced Photonics Research*, 2022, 3 (11): 2200110.
[30] QIU Y H, CHEN S X, HOU Z Y, et al. Chiral metasurface for near-field imaging and far-field holography based on deep learning [J]. *Micromachines*, 2023, 14(4): 789.
[31] WANG H P, CAO D M, et al. Inverse design of metasurfaces with customized transmission characteristics of frequency band based on generative adversarial networks [J]. *Optics Express*, 2023, 31(23): 37763.
[32] AN S S, ZHENG B W, TANG H, et al. Multifunctional metasurface design with a generative adversarial network [J]. *Advanced Optical Materials*, 2021, 9(5): 2001433.
[33] MIRZA M, OSINDERO S. Conditional generative adversarial nets[EB/OL]. (2014-11-06)[2024-02-05]. https://arxiv.org/pdf/1411.1784.
[34] GULRAJANI I, AHMED F, ARJOVSKY M, et al. Improved training of Wasserstein GANs [EB/OL]. (2017-12-25)[2024-02-05]. https://arxiv.org/pdf/1704.00028.
[35] MA T G, TOBAH M, WANG H Z, et al. Benchmarking deep learning-based models on nanophotonic inverse design problems[J]. *Opto-Electronic Science*, 2022, 1(1): 210012.

基于生成对抗网络模型的双波长双聚焦超透镜设计

刘港成[1]，王军凯[1]，林　森[1]，伍滨和[1*]，王春瑞[1]，周　健[2]，孙　浩[2*]

1. 东华大学 物理学院，上海 201620

2. 中国科学院 上海微系统与信息技术研究所，上海 200050

摘　要：多焦点超透镜在光通信、光学成像和显微光学等领域具有重要价值，然而其设计具有极大的挑战性。近年来，深度学习方法为光学平面器件的设计提供了新的解决方案。该文提出了一种使用生成对抗网络（generative adversarial network，GAN）来实现双波长下不同聚焦位置的超透镜设计方法。该方法包括前向网络和逆向设计网络。前者用于快速预测超原子结构的光学响应，后者自动生成符合需求的超原子结构。与传统搜索方法相比，逆向设计网络在设计双波长双聚焦超透镜时具有更高的准确性和效率。这些结果将为可调波长超透镜的设计提供思路和方法，突显了深度学习在光学器件设计中的潜力。

关键词：生成对抗网络；超透镜；前向网络；逆向设计